

Japan) was added to prevent algae or limescale which are generated in the circuit.

For measurement, a data acquisition system (PowerLab; ADInstruments Japan, Aichi, Japan) was used. The analog-to-digital sampling frequency for each pressure and flow rate channel was 200 Hz.

## RESULTS

### Valvular function

The LVP, AoP, and flow rate waveforms for each biovalve (A, B, C) at a HR of 70 bpm are shown in Fig. 4a–c. The mean AoPs for biovalve A, B, and C were 80, 105, and 105 mm Hg, and the mean flow rates were 4.6, 5.5, and 5.5 L/min, respectively. From the flow rate waveforms, significant diastolic regurgitation was observed for biovalve A; however, there was almost no regurgitation for biovalves B and C. The regurgitation rates for biovalves A, B, and C were 46.3, 2.6, and 3.3%, respectively. Table 2 shows the pressures and flow rates for each biovalve and the two commercially available valves at each HR. In this experiment, the stroke volume of the pulsatile pump, the compliance of the closed chamber, and fluid resistance were adjusted to maintain an average AoP of  $100 \pm 20$  mm Hg as the HR was increased. The mean flow rate for biovalve B and C ranged from 5.5 to 8.9 L/min at a mean AoP of 100 mm Hg as the HR was increased from 70 to 120 bpm. Equivalent pressures and flow rates were also obtained for the other two commercially available valves. The average regurgitation rate of biovalve B and C was approximately 3.0%. The regurgitation rate of biovalve B and C was equivalent to that obtained for the biological and mechanical valves at each HR.

### Long-term continuous operation

Figure 5 shows the result of the long-term, continuous operation experiment. Each plot shows the mean values of LVP, AoP, flow rate, and regurgitation rate, averaged for 1 min each day under steady-state circulatory conditions. The durability test demonstrated that even after biovalve C was pulsated more than four million times (HR, 70 bpm; mean flow rate, 5.0 L/min; mean AoP, 92 mm Hg), stable continuous operation was possible without excessive reduction of flow rate or bursting. The regurgitation rate on the first day was approximately 6%. The regurgitation rate was <10% in the early stages (after 2 days), but it increased gradually thereafter. The regurgitation rate after 40 days reached approximately 15%. Figure 6 shows the LVP, AoP, and flow waveforms on the first day and after 40 days. Although the pulsatility in each

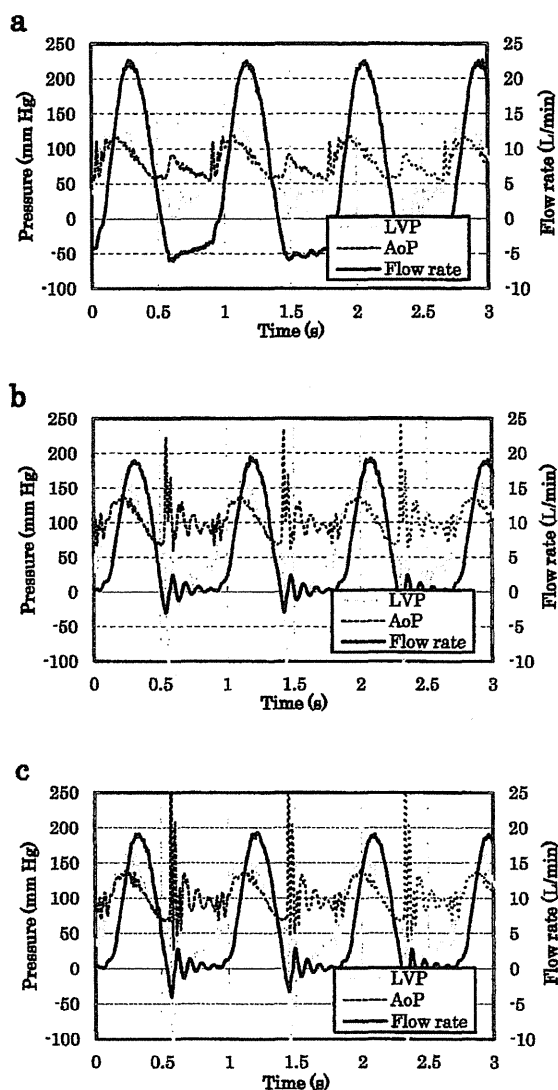


FIG. 4. LVP, AoP, and flow rate waveforms for each biovalve at 70 bpm in the pulsatile circulation circuit. (a) Biovalve A, (b) Biovalve B, (c) Biovalve C.

waveform did not change, the amount of diastolic regurgitation increased after 40 days.

## DISCUSSION

A mock circulatory circuit was used to evaluate function and durability of the biovalve under the type of pulsatile load that exists in the systemic circulation. This *in vitro* test was performed to assess whether the biovalve can be used as the aortic valve. Recently, several valves such as prosthetic heart valves or porcine valves were evaluated using the

**TABLE 2.** The HR characteristics of each biovalve, the biological valve, and the mechanical valve

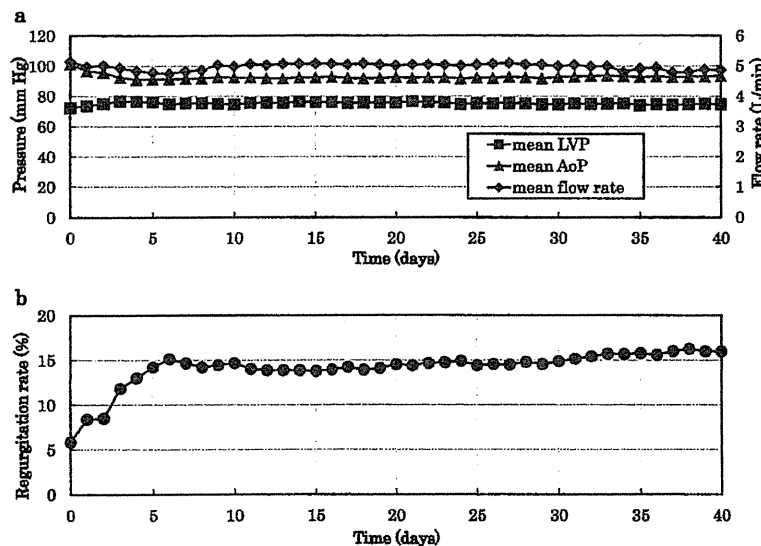
Parameters	Biovalve A	Biovalve B	Biovalve C	Biological valve	Mechanical valve
Heart rate (bpm)	70–120	70–120	70–120	70–120	70–120
Mean flow rate (L/min)	4.64–7.08	5.52–8.96	5.48–8.89	5.52–8.57	5.52–8.73
Mean LVP (mm Hg)	75.48 ± 6.07	74.86 ± 3.80	74.91 ± 3.08	88.56 ± 8.36	83.96 ± 8.31
Mean AoP (mm Hg)	82.17 ± 4.07	99.15 ± 8.40	98.54 ± 8.49	111.94 ± 3.04	115.84 ± 3.87
Mean regurgitation (L/min)	1.72 ± 0.26	0.18 ± 0.02	0.25 ± 0.05	0.15 ± 0.01	0.21 ± 0.01
Regurgitation rate (%)	26.12 ± 10.90	2.49 ± 0.22	3.40 ± 0.12	2.12 ± 0.36	2.97 ± 0.33

[Corrections added on 20 November 2013, after first online publication: Heart rate values in the first row have been changed from 7–120 to 70–120.]

pulsatile mock circulation system (10–13). Although a mock circulation loop does not replace *in vivo* trials, we believe that the use of the pulsatile mock circulation system in this study was an effective means of evaluating valve function before *in vivo* tests or clinical studies.

The influence of leaflet length on valvular function in the biovalves was examined. Regurgitation was observed during the diastolic phase of the cardiac cycle with biovalve A, whereas there was almost no regurgitation with biovalve B. We believe that biovalve B was able to maintain AoP during the diastolic phase because the coaptation area of leaflets was increased by extending the leaflets of the biovalve in an axial direction. The effectiveness of the extended leaflets in biovalve B against the pressures of the systemic circulation was confirmed. The influence of the presence or absence of sinuses of Valsalva in the biovalve under the pulsatile loading conditions that exist in the systemic circulation was also assessed. The results showed that there was no influence of the sinuses of Valsalva on the pressure or flow

rate waveforms, or the mean regurgitation rate. Vortex flow in the sinuses of Valsalva plays an important role in the closure of native semilunar valves at the end of systole and in facilitating coronary flow during systole (14). Valves lacking the sinuses of Valsalva close only passively due to the backflow of blood (15). Although biovalve C did not have the sinuses of Valsalva, its regurgitation rate was not different from the regurgitation rate of biovalve B. Therefore, we believe that the sinuses of Valsalva may not be necessary if the coaptation area of leaflets in the biovalve is wide enough. Each biovalve was compared with conventional biological and mechanical valves over a practical range of HRs. There were no large differences in mean LVP, mean AoP, mean flow rate, or the mean regurgitation rate among four valves (biovalve B, biovalve C, biological valve, and mechanical valve) as the HR varied from 70 to 120 bpm. These results suggest that the biovalve B and C functioned as well as the two commercially available valves, at least on a short-term basis. In this study, evaluation of biovalve was performed

**FIG. 5.** Continuous operation of biovalve C for 40 days. (a) Mean LVP, AoP, and flow rate for biovalve C over time. (b) Regurgitation rate of biovalve C over time.

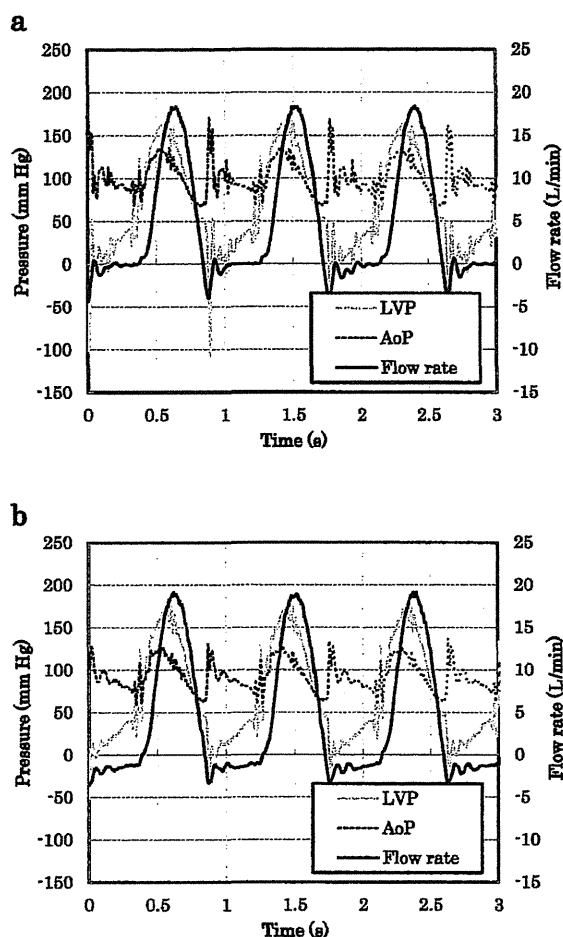


FIG. 6. LVP, AoP, and flow rate waveform on the first day and after 40 days in the long-term, continuous operation experiment in Fig. 5. (a) First day. (b) After 40 days.

using the pulsatile circulation circuit. Saline which has a different viscosity from blood was selected as the working fluid for prevention of injury in biovalves made of natural tissues. However, it was considered that the evaluation of the valvular functions of biovalves in comparison to two commercially available valves to the pulsatile pressure loads that simulated the systemic circulation conditions was achieved in this circulation circuit. In the near future, we will perform a detailed examination of the valve behavior or internal flow pattern of the biovalve under flow conditions similar to a living body.

In terms of continuous biovalve operation, the regurgitation was approximately 6% in the early phase, and it increased gradually thereafter to approximately 15%. Normally, the connective tissue

of the biovalve becomes infiltrated with cells, and the wall thickness of the conduit and sinus of Valsalva significantly increases after implantation in vivo. In this study, the biovalve was evaluated under very severe conditions because cell-free saline was used as the working fluid in the mock circulation system. We believe that the regurgitation of biovalve C increased after 40 days because the mechanical strength of the biovalve decreases without cell invasion during continuous operation. It was reported that pulsatile flow loading in vitro for 2 days caused the sparse, randomly oriented collagen fibers in biotubes to become dense and oriented in the regular circumferential direction (16). The biotubes used in that study were fabricated with the same technology as the biovalves used in the present study, in terms of collagen structures and mechanical properties (16). Therefore, if cells infiltrate the connective tissue of the biovalve in the early phase of low regurgitation, it may be possible to prevent the increase in regurgitation. In future studies, evaluation of biovalve durability including cell invasion will be necessary to validate the usefulness of the biovalve. In the present study, the developed biovalve maintained a regurgitation rate of about 15% without cell invasion into the connective tissue. However, long-term durability of the biovalve is insufficient compared with mechanical valves or biological valves in the case where cells do not invade. Therefore, not only the improvement of mechanical properties which depend on cell invasion but also the improvement in the mechanical durability of the biovalve itself is required in order to obtain the durability equivalent to the mechanical valves or biological valves. The results of valvular function testing showed that the expansion of coaptation area of leaflets was effective against regurgitation. Therefore, further increasing the coaptation area of the leaflets might help prevent regurgitation. One of the advantages of using "in-body tissue architecture technology" is that a biovalve of any arbitrary form can be developed by the appropriate design of the molds. It might be possible to develop optimally shaped leaflets in a biovalve to produce good valvular function and durability, even without cell invasion. The biovalve developed using "in-body tissue architecture technology" has the potential to become the most effective replacement therapy for severe valvular heart disease.

## CONCLUSIONS

We evaluated the valvular function and durability of the biovalve in vitro. The biovalve was compared with commercially available valves under conditions

that simulated the systemic circulation. The leaflet size, which is responsible for the coaptation area, is important to prevent increases in biovalve regurgitation during long-term operation, and the sinuses of Valsalva may be unnecessary for optimal biovalve function. The developed biovalve demonstrated good valvular function and durability and may be potentially useful for aortic valve replacement.

**Acknowledgment:** The present study was supported by Grants-in-Aid for Challenging Exploratory Research (no. 20332405) from the Ministry of Education, Culture, Sports, Science and Technology of Japan.

## REFERENCES

1. Tokunaga S, Tominaga R. Artificial valves "up to date" in Japan. *J Artif Organs* 2010;13:77–87.
2. Mendelson K, Schoen FJ. Heart valve tissue engineering: concepts, approaches, progress, and challenges. *Ann Biomed Eng* 2006;34:1799–819.
3. Nakayama Y, Yamanami M, Yahata Y, et al. Preparation of a completely autologous trileaflet valve-shaped construct by in-body tissue architecture technology. *J Biomed Mater Res B Appl Biomater* 2009;91:813–8.
4. Yamanami M, Yahata Y, Tajikawa T, et al. Preparation of in-vivo tissue-engineered valved conduit with the sinus of Valsalva (type IV biovalve). *J Artif Organs* 2010;13:106–12.
5. Yamanami M, Yahata Y, Uechi M, et al. Development of a completely autologous valved conduit with the sinus of Valsalva using in-body tissue architecture technology: a pilot study in pulmonary valve replacement in a beagle model. *Circulation* 2010;122(11 Suppl.):S100–6.
6. Nakayama Y, Yahata Y, Yamanami M, et al. A completely autologous valved conduit prepared in the open form of trileaflets (type VI biovalve): mold design and valve function in vitro. *J Biomed Mater Res B Appl Biomater* 2011;99:135–41.
7. Takewa Y, Yamanami M, Kishimoto Y, et al. In vivo evaluation of an in-body, tissue-engineered, completely autologous valved conduit (biovalve type VI) as an aortic valve in a goat model. *J Artif Organs* 2013 16:176–84.
8. Nakayama Y, Takewa Y, Sumikura H, et al. In vitro and in vivo performance of a completely autologous aortic valved conduit (BIOVALVE Type VII) prepared by in body tissue architecture technology using a novel separable mold. *Circulation* 2012;126:A8910.
9. Sumikura H, Homma A, Ohnuma K, et al. Development and evaluation of endurance test system for ventricular assist devices. *J Artif Organs* 2013 16:138–48.
10. Suzuki I, Shiraishi Y, Yabe S, et al. Engineering analysis of the effects of bulging sinuses in a newly designed pediatric pulmonary heart valve on hemodynamic function. *J Artif Organs* 2012;15:49–56.
11. Vismara R, Fiore GB, Mangini A, et al. A novel approach to the in vitro hydrodynamic study of the aortic valve: mock loop development and test. *ASAIO J* 2010;56:279–84.
12. Rahmani B, Tzamtzis S, Ghanbari H, Burriesci G, Seifalian AM. Manufacturing and hydrodynamic assessment of a novel aortic valve made of a new nanocomposite polymer. *J Biomech* 2012;45:1205–11.
13. Parravicini R, Cocconcelli F, Verona A, Parravicini V, Giuliani E, Barbieri A. Tuna cornea as biomaterial for cardiac applications. *Tex Heart Inst J* 2012;39:179–83.
14. Kunzelman KS, Grande KJ, David TE, Cochran RP, Verrier ED. Aortic root and valve relationships. Impact on surgical repair. *J Thorac Cardiovasc Surg* 1994;107:162–70.
15. Ohta Y, Kikuta Y, Shimooka T, Mitamura Y, Yuhta T, Dohi T. Effect of the sinus of Valsalva on the closing motion of bileaflet prosthetic heart valves. *Artif Organs* 2000;24:309–12.
16. Huang H, Zhou YM, Ishibashi-Ueda H, et al. In vitro maturation of "biotube" vascular grafts induced by a 2-day pulsatile flow loading. *J Biomed Mater Res B Appl Biomater* 2009;91:320–8.



# In-body tissue-engineered aortic valve (Biovalve type VII) architecture based on 3D printer molding

Yasuhide Nakayama,<sup>1</sup> Yoshiaki Takewa,<sup>2</sup> Hirohito Sumikura,<sup>2</sup> Masashi Yamanami,<sup>1,3</sup> Yuichi Matsui,<sup>1,4</sup> Tomonori Oie,<sup>1</sup> Yuichiro Kishimoto,<sup>2</sup> Mamoru Arakawa,<sup>2</sup> Kentaro Ohmuma,<sup>2</sup> Tsutomu Tajikawa,<sup>4</sup> Keiichi Kanda,<sup>3</sup> Eisuke Tatsumi<sup>2</sup>

<sup>1</sup>Division of Medical Engineering and Materials, National Cerebral and Cardiovascular Center Research Institute, Osaka, Japan

<sup>2</sup>Department of Artificial Organs, National Cerebral and Cardiovascular Center Research Institute, Osaka, Japan

<sup>3</sup>Department of Cardiovascular Surgery, Kyoto Prefectural University of Medicine, Kyoto, Japan

<sup>4</sup>Department of Mechanical and Systems Engineering, Kansai University, Osaka, Japan

Received 27 November 2013; revised 15 March 2014; accepted 12 April 2014

Published online 00 Month 2014 in Wiley Online Library (wileyonlinelibrary.com). DOI: 10.1002/jbm.b.33186

**Abstract:** In-body tissue architecture—a novel and practical regeneration medicine technology—can be used to prepare a completely autologous heart valve, based on the shape of a mold. In this study, a three-dimensional (3D) printer was used to produce the molds. A 3D printer can easily reproduce the 3D-shape and size of native heart valves within several processing hours. For a tri-leaflet, valved conduit with a sinus of Valsalva (Biovalve type VII), the mold was assembled using two conduit parts and three sinus parts produced by the 3D printer. Biovalves were generated from completely autologous connective tissue, containing collagen and fibroblasts, within 2 months following the subcutaneous embedding of the molds (success rate, 27/30). *In vitro* evaluation, using a pulsatile circulation circuit, showed excellent valvular function with a durability of at least 10 days. Interposed

between two expanded polytetrafluoroethylene grafts, the Biovalves ( $N=3$ ) were implanted in goats through an apico-aortic bypass procedure. Postoperative echocardiography showed smooth movement of the leaflets with minimal regurgitation under systemic circulation. After 1 month of implantation, smooth white leaflets were observed with minimal thrombus formation. Functional, autologous, 3D-shaped heart valves with clinical application potential were formed following in-body embedding of specially designed molds that were created within several hours by 3D printer. © 2014 Wiley Periodicals, Inc. *J Biomed Mater Res Part B: Appl Biomater* 00B:000–000, 2014.

**Key Words:** tissue engineering, heart valve, 3D printer, connective tissue, surgery

**How to cite this article:** Nakayama Y, Takewa Y, Sumikura H, Yamanami M, Matsui Y, Oie T, Kishimoto Y, Arakawa M, Ohmuma K, Kanda K, Tatsumi E. 2014. In-body tissue-engineered aortic valve (Biovalve type VII) architecture based on 3D printer molding. *J Biomed Mater Res Part B* 2014:00B:000–000.

## INTRODUCTION

Surgical alternatives for end-stage valvular heart disease consist of the application of either mechanical or biological prostheses, both of which have significant limitations.<sup>1</sup> Although mechanical valves have a functional life span of at least 25 years, they are associated with the need for life-long anticoagulation and the concomitant risks of thromboembolism and bleeding. Biological prostheses, generally, have better hemodynamic characteristics and do not require long-term anticoagulation, but are associated with progressive tissue deterioration. Therefore, tissue-engineering techniques may play a prominent role in the future development of heart valve replacements. Much of the research designed to create *in vitro* tissue-engineered heart valves has focused on the scaffold materials, culturing of cells, and the use of appropriate seeding and preconditioning protocols.<sup>2,3</sup> However, the mechanical integrity of the replacement valves and their abil-

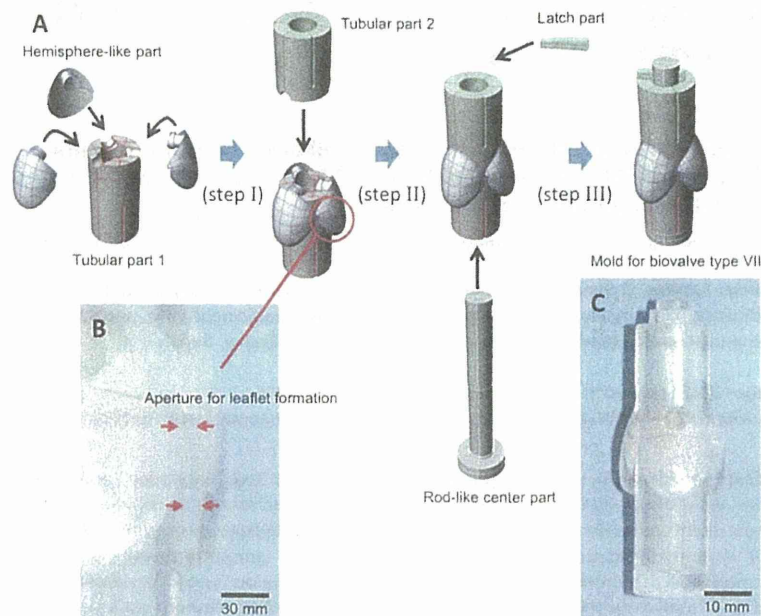
ity to withstand systemic pressures depends on the neo-tissue. Therefore, the clinical utility of these autologous tissue-engineered heart valves is limited, particularly in growing children.

The medical and engineering relevance of computer-based three-dimensional (3D) procedures—known as 3D printing—is increasing, which increases the potential of rapid prototyping techniques.<sup>4,5</sup> The technology presented in this paper is based on the principle of building 3D models, layer by layer, and enables the direct manufacturing of precise, complex-shaped implants using biocompatible or biodegradable materials from computerized data in several medical areas.<sup>6–9</sup>

As a feasible, regenerative medicine approach, we developed completely autologous valved conduits, named Biovalves,<sup>10–12</sup> without any artificial scaffolds, through the use of “in-body tissue architecture” technology. This autologous

**Correspondence to:** Y. Nakayama (e-mail: ny@ncvc.go.jp)

Contract grant sponsor: Ministry of Education, Culture, Sports, Science, and Technology of Japan; contract grant number: B23360374



**FIGURE 1.** (A) Schematic diagram of the assembly process of seven parts (three hemisphere-like parts, two tubular parts, rod-like center part and latch part) for the mold in three steps. (B) Photo of the aperture (between red arrows) for leaflet formation. (C) Photo of the assembled mold. [Color figure can be viewed in the online issue, which is available at [wileyonlinelibrary.com](http://www.interscience.wiley.com).]

method is based on the phenomenon of tissue encapsulation of foreign materials implanted in living bodies.<sup>13</sup> The technology offers the following advantages: the developed tissue prostheses are non-toxic, particularly non-carcinogenic, and can be fabricated in a wide range of shapes and sizes to suit the needs of individual recipients. In addition, the prostheses, without any artificial materials, possess the characteristics of their natural counterparts, including anticoagulation, self-repair, tissue regeneration, and growth adaptability. These prostheses do not require complex *in vitro* cell management procedures or exceptionally clean laboratory facilities, both of which are expensive and labor-intensive over long periods.

In an early development stage, Biovalves were prepared in small size animal models such as rats or beagle dogs, which are less relevant for heart valve testing. In the present paper, we used a 3D printer to produce a Biovalve mold. The clinical feasibility of the Biovalves obtained from the mold was evaluated by implanting the aortic Biovalve in a big size animal using a goat model for estimation of aortic valvular performance in a human systemic circulation condition, after evaluating their function and durability *in vitro*.

## MATERIALS AND METHODS

### Animal studies

The animal studies were performed in accordance with the "Guide for the Care and Use of Laboratory Animals," published by the United States National Institutes of Health (NIH Publication No. 85-23, revised 1996) under a protocol approved by the National (Japan) Cerebral and Cardiovascular Center Research Institute Committee (No. 12002).

### Mold preparation

Seven fine plastic parts [Figure 1(A)], produced using a 3D digital printer (Projet HD3000, 3D Systems, Rock Hill, SC), were assembled to create the molds [Figure 1(C)]. First, three small hemispherical parts (Figure 2) for the sinus of the Valsalva were fastened between the two tubular parts of the conduit (diameter, 16 mm), with a small, 1-mm aperture between the three hemispherical parts and the tubular part [steps I and II in Figure 1(A)]. Second, the combined parts (height, 5 cm) were fixed with a central rod and a latch to obtain the final mold (step III). The mold was based on the geometry of a goat aortic valve and was designed for the formation of the leaflets that are separated from each other in the open position.

### Biovalve preparation

A total of 30 molds were placed into dorsal subcutaneous pouches in 10 goats (age, 1–2 years; body weight, 40–50 kg), under general anesthesia induced with 10 mg/kg of ketamine and maintained with 1–3% isoflurane. The leaflet formation at the three apertures was non-invasively observed using a capsule endoscope<sup>14</sup> (EC Type 1, Olympus, Tokyo, Japan), present in one of the tubular parts of the mold [Figure 3(A)]. Two months later, after complete encapsulation with connective tissue, the structures were harvested [Figure 3(B)]. Biovalves, with three protrusions resembling the sinuses of Valsalva [Figure 3(E)], were obtained by removing all of the parts from the ends of the developed tubular tissue. The three membranous leaflets had formed in the open position inside the conduit. Each leaflet had an area of 2.4 cm<sup>2</sup>, with a height

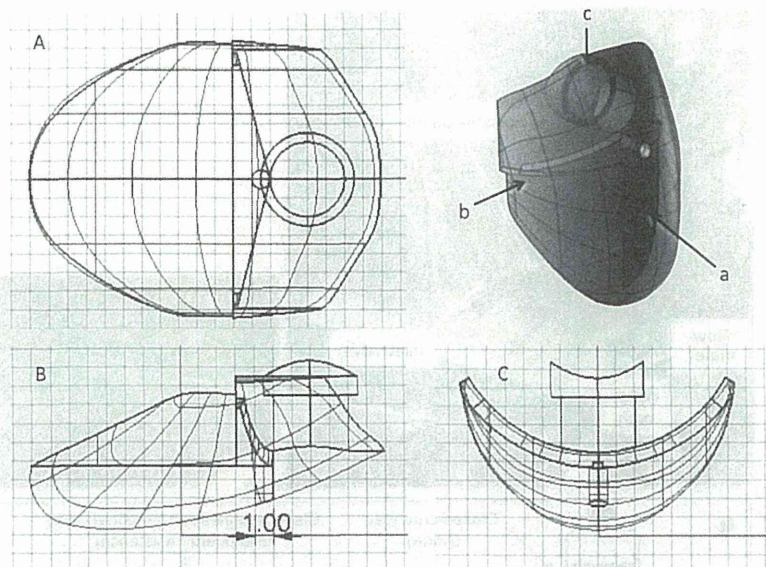


FIGURE 2. Projection drawings of the hemisphere-like parts used in the preparation of the leaflets and the sinus of Valsalva (A, front view; B, side view; C, top view).

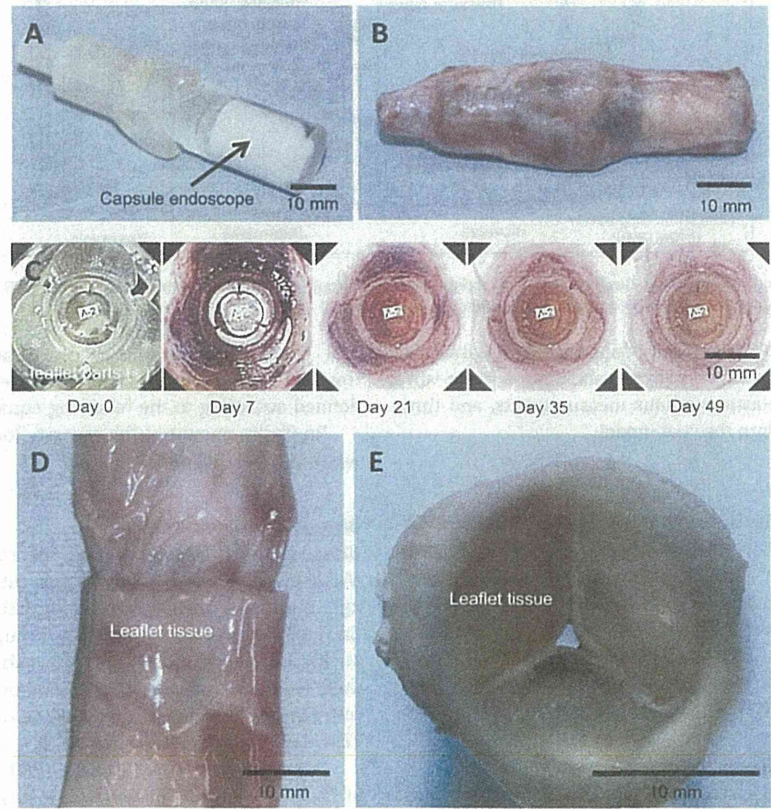
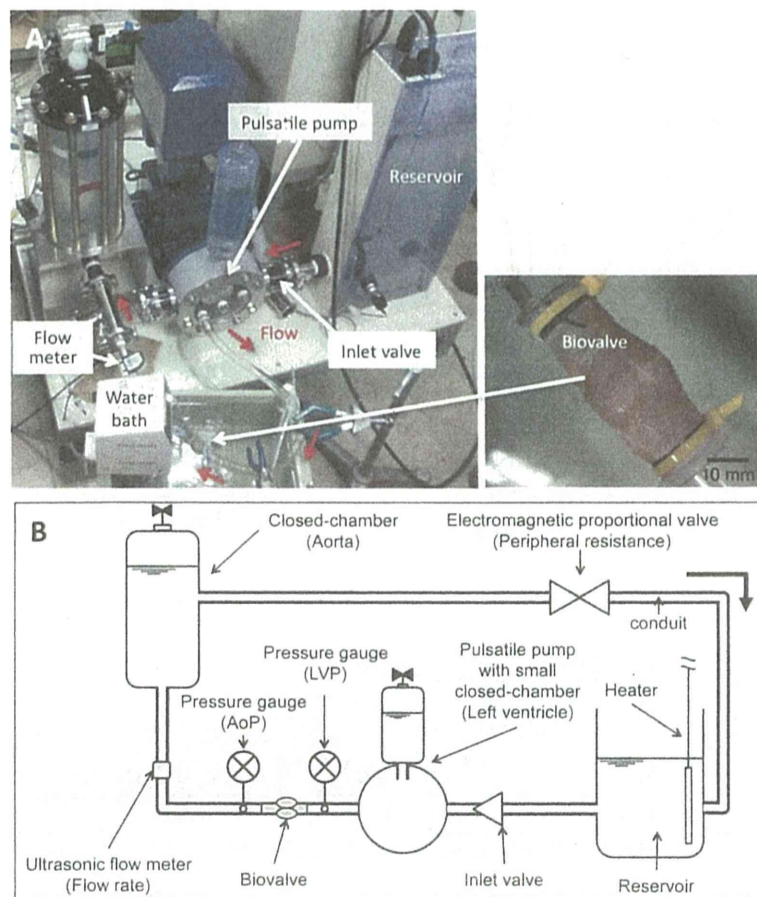


FIGURE 3. Photos of the preparation mold, impregnated with a capsule endoscope, (A) before and (B) after encapsulation. (C) The leaflet formation process at the aperture of the mold observed using a capsule endoscope non-invasively. Photos of (D) the luminal surface of the Biovalve and (E) the closed form with three protrusions resembling the sinus of Valsalva. [Color figure can be viewed in the online issue, which is available at [wileyonlinelibrary.com](http://wileyonlinelibrary.com).]





**FIGURE 4.** (A) Photo and (B) schematic diagram of the pulsatile circulation circuit connected with the Biovalve in a 37°C water bath. [Color figure can be viewed in the online issue, which is available at [wileyonlinelibrary.com](http://wileyonlinelibrary.com).]

of 1.7 cm. Of the 27 successfully constructed Biovalves, we randomly selected five for *in vitro* evaluations of their valve functions, five for elastic modulus measurements, and three for transplantation into the goat model.

#### Elastic modulus

The tensile strengths of the Biovalve tissues were measured using a uniaxial tensile-testing apparatus (Rheoner II, Yamaden, Tokyo, Japan). Each sample was cut into rectangular strips (5-mm wide) and fixed to the upper and lower grips (initial length, 5 mm). A tensile load was applied by moving the lower grip at a rate of 0.05 mm/s until failure, that is, tissue rupture. The maximum elastic modulus before rupture was obtained from the slope of the stress-strain curve.

#### *In vitro* functionality tests

Biovalves were connected to a pulsatile circulation circuit (LaboHeart NCVC, IWAKI, Tokyo, Japan; Figure 4). The valvular functions of the Biovalves were examined at 37°C, under pulsatile conditions designed to simulate human systemic circulation (pressure, 49–129 mmHg; beat rate, 70–

120 beats/min). The mean regurgitation was calculated from 10 beat cycles. The degree of regurgitation (Re) was defined according to the following equation.

$Re (\%) = \text{amount of the reverse flow} / \text{amount of the forward flow} \times 100$

#### Biovalve implantation

Biovalves were implanted into the previously used goats ( $N = 3$ ), which were premedicated with ketamine (10 mg/kg), intubated, and anesthetized with isoflurane (1–3%). Each animal's heart was exposed through a left thoracotomy at the fifth subcostal region. Both ends of the Biovalve conduit were anastomosed to expanded polytetrafluoroethylene (ePTFE) grafts (internal diameter, 14 mm  $\times$  20 cm; GORE-TEX, W. L. Gore & Associates, Newark, DE).

After systemic heparinization (200 U/kg), the distal end of each composite graft was anastomosed to the descending aorta in an end-to-side manner under a partially occluding clamp. A felt cuff was sewn to the left ventricular apex. The apex was cored with a 19-mm, custom-made, ventricular coring device. Thereafter, an apical-left ventricle connector,

composed of a custom-made, stainless steel conduit and a 14-mm ePTFE graft, were inserted through the felt cuff into the apex and tied to the felt cuff. To complete the bypass, the grafted part of the connector was sewn, in an end-to-end manner, to the proximal end of the composite graft, thus interposing the Biovalve. Finally, the descending aorta was ligated, with vessel tape, at the proximal portion of the anastomosis to ensure that the blood flow to the abdominal aorta was completely supplied via the apico-aortic bypass that incorporated the Biovalve. Postoperative systemic anticoagulation was maintained with oral administration of warfarin sodium (3 mg/day) and aspirin (81 mg/day) for 1 month.

#### *In vivo* functionality tests

Immediately after implantation, angiography was used to evaluate the valvular function; weekly transthoracic Doppler echocardiography was utilized thereafter. Bypass flow was continuously monitored using electromagnetic and ultrasonic flow meters; the probes were attached around the ePTFE grafts.

#### Tissue analyses

The tissue compositions of the Biovalves, before and after implantation, were assessed by histological examination. Samples were fixed in phosphate-buffered formalin and embedded in paraffin; 5- $\mu$ m, longitudinally sliced sections were examined for general tissue morphology (hematoxylin-eosin stain) and the presence of collagen (Masson trichrome stain) and elastin (Elastica-van Gieson stain).

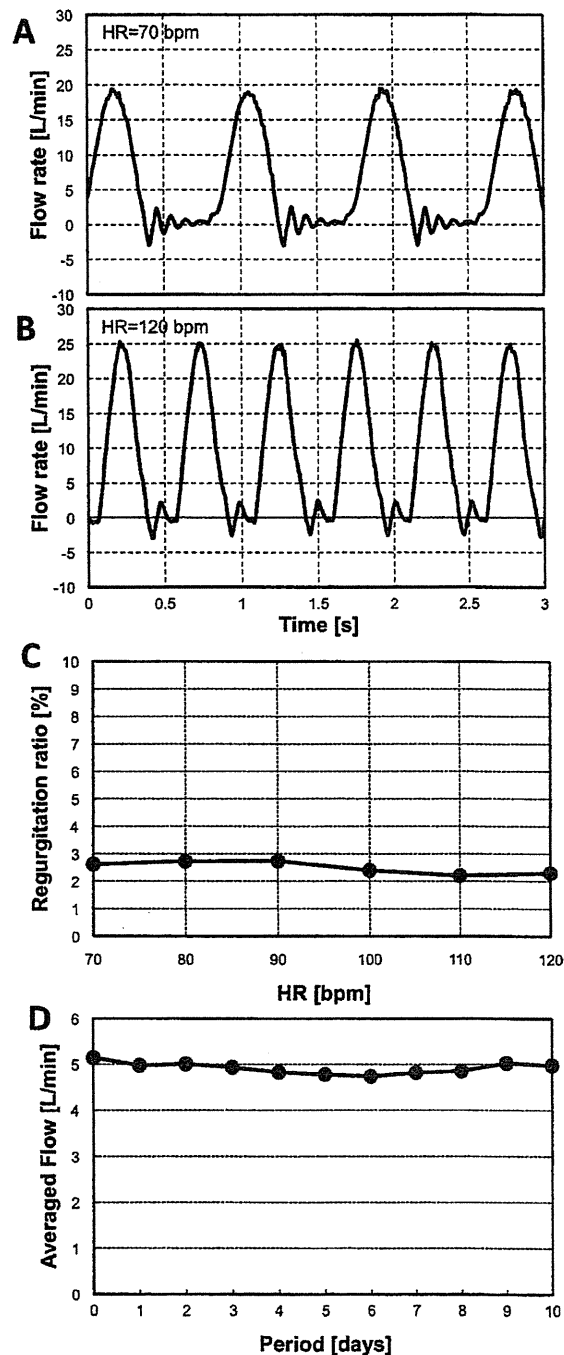
#### Statistics

Quantitative data are presented as means  $\pm$  standard deviation.

### RESULTS

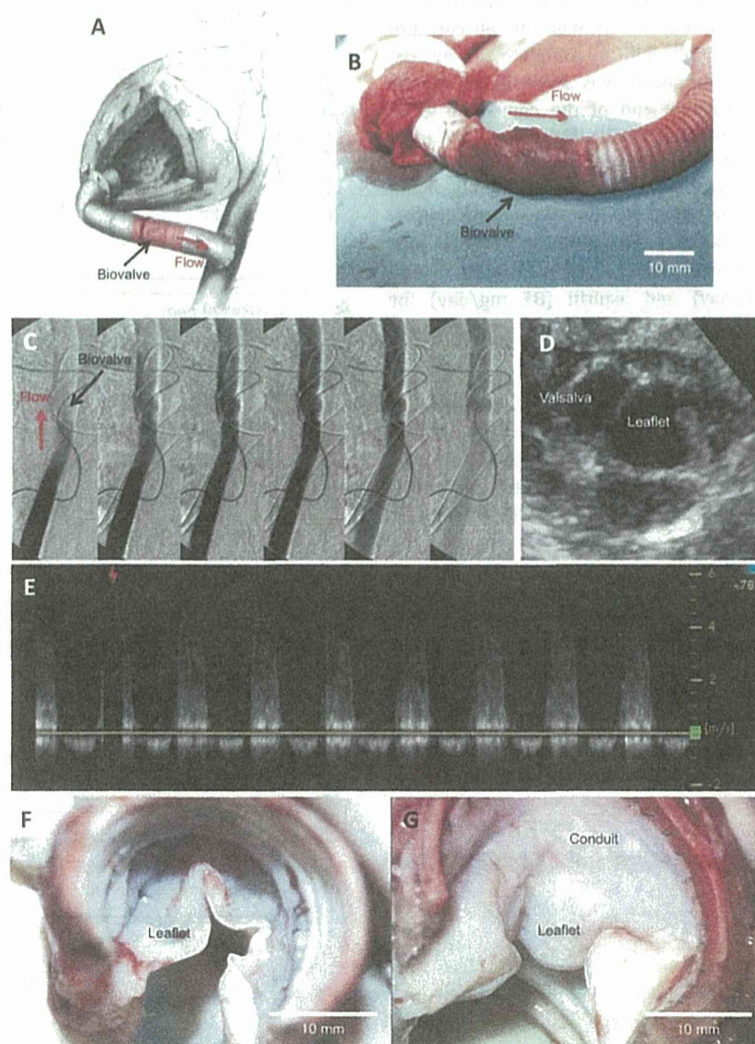
#### Preparation of biovalves

Figure 1 shows schematic diagram of the assembly process of the fine plastic mold parts. All parts, including the complex-shaped hemispherical components (Figure 2), were precisely produced by 3D printer within several hours [Figure 1(A)]. The hemispherical parts were used for the formation of the leaflets and the sinus of Valsalva. These were placed on a tubular section prepared by connecting the two rod-like parts [steps I and II in Figure 1(A)] with a small aperture for leaflet formation [Figure 1(B)]. The combined components were fixed with a rod-like part and a latch [step III in Figure 1(A)]. The resultant molds [Figure 1(C)] were completely encapsulated with autologous connective tissues during the preparation process [Figure 3(B)]. The molds, impregnated in the developed tissue, were easily removed by separating the assembled parts without any resultant tissue damage. Thin membranous tissues developed at the three apertures between the tubular part and the three hemispherical parts, forming three leaflets inside the conduit tissue [Figure 3(D)]. When the leaflet tissues were blown, a closed Biovalve was obtained [Figure 3(E)].



**FIGURE 5.** Pulsatile flow waveforms of Biovalves with a pulsatile flow rate of (A) 70 beats/min and (B) 120 beats/min. (C) Regurgitation ratio change under different heart rate from 70 to 120 bpm. (D) Averaged flow change up to 10 days.

Observation of the leaflet formation, using a capsule endoscope [Figure 3(A)], revealed that tissue ingrowth into the apertures occurred gradually, with concurrent capillary



**FIGURE 6.** (A) Schematic picture of the implantation model via an apico-aortic bypass method. (B) Photo of the Biovalve implanted by interposing between artificial grafts. (C) Intraoperative angiography immediately after implantation. Leaflet observation at circumferential section (D) and flow measurement (E) by transthoracic doppler echocardiography. Macroscopic photos of Biovalves after 1 month of implantation: views from the aortic side (F) and the ventricular side (G). [Color figure can be viewed in the online issue, which is available at [wileyonlinelibrary.com](http://wileyonlinelibrary.com).]

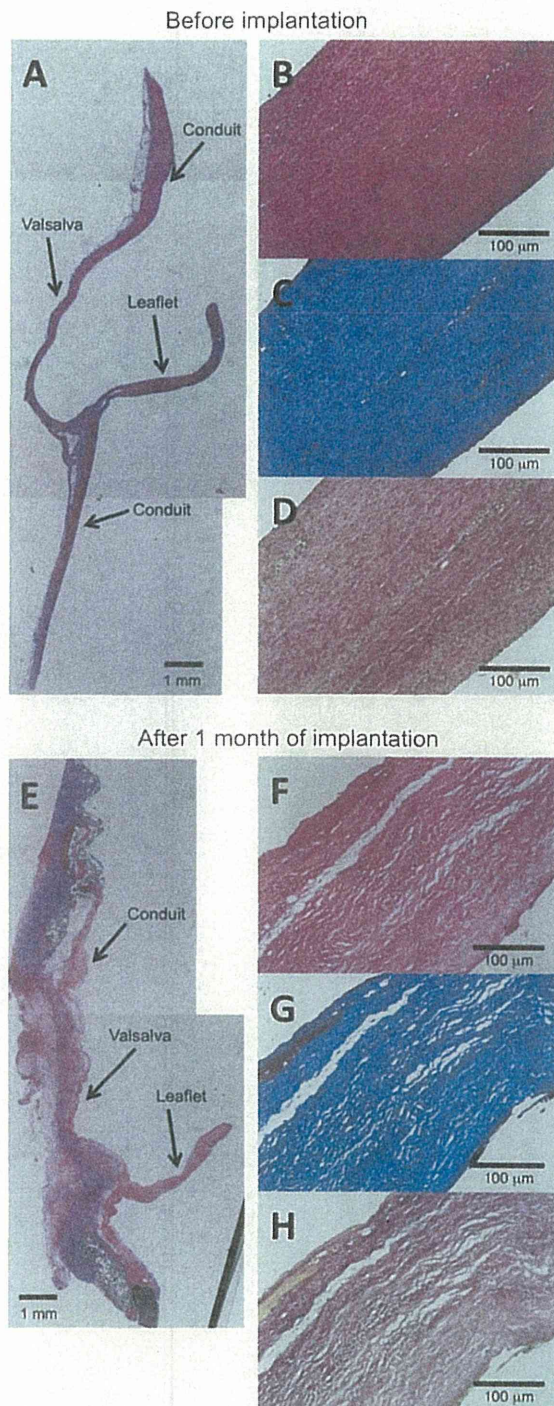
formation [Figure 3(C)]. After being implanted for 49 days, the apertures were completely replaced by autologous connective tissues to form leaflet tissues in the molds. The success rate of Biovalve preparation using this method was 90% (27/30). In two molds collapse of the hemispherical parts in the molds occurred, possibly due to the lack of strength of the mold material. In 1 mold, inflammation was observed due to infection. The 27 usable Biovalves had well-formed, tubular-shapes, with three protrusions resembling the sinus of Valsalva; the quality of the Biovalves appeared to be almost identical [Figure 3(E)]. Inside the conduit, three separate membranous leaflets were present and were connected at the commissure without an aperture.

The maximum elastic modulus of the leaflet part of Biovalves was  $1083 \pm 288$  kPa, which was very close to that of a natural goat leaflet ( $1097 \pm 389$  kPa). The conduit part of each Biovalve was significantly more robust ( $2800 \pm 610$  kPa)—approximately six-times that of the goat aorta ( $494 \pm 169$  kPa).

#### ***In vitro* valve function**

Valvular functioning of Biovalves was examined using a pulsatile circuit (Figure 4). Figures 5A, B indicate the typical flow waveforms, compared at 70 and 120 beats/min, respectively, with a mean flow rate of 5.0 L/min and an aortic pressure of 129–49 (mean, 82.2) mmHg. For all





**FIGURE 7.** Tissue morphology of Biovalves (A–D) before and (E–H) after 1 month of implantation. A, B, E, and F; hematoxylin and eosin staining, C and G; Masson's trichrome stain; D and H; Elastica-van Gieson stain. The upper portion is the distal side and the lower portion is the proximal side in all the images. [Color figure can be viewed in the online issue, which is available at [wileyonlinelibrary.com](http://wileyonlinelibrary.com).]

Biovalves ( $N = 5$ ), regurgitation during the diastolic phase was  $<3\%$  [Figure 5(C)]. In addition, the mean flow rate ( $4.9$  L/min) was maintained for at least for 10 days in a saline solution at  $37^\circ\text{C}$  [Figure 5(D)].

#### *In vivo* application

During interposed implantation of the Biovalve into an apico-aortic bypass via end-to-end anastomosis with ePTFE grafts [Figure 6(A)], the surgical handling of Biovalves was found to be equivalent to that of native tissues. After declamping, the connected Biovalve pulsated with minimal bleeding [Figure 6(B)]. Intraoperative angiography of the bypass circuit after implantation, revealed protrusions, similar to those of the sinus of Valsalva, with leaflets that opened and closed smoothly; moreover, there was good blood flow and minimal regurgitation [Figure 6(C)]. Up to 1 month after implantation, transthoracic echocardiographic examinations revealed protrusions similar to those of the sinus of Valsalva [Figure 6(D)]. Doppler echocardiography did not yield substantial evidence of stenosis or regurgitation. The Biovalves showed good forward flow during the systolic phase and trivial regurgitation during the diastolic phase [Figure 6(E)]. Bypass flow was maintained at  $2.6 \pm 1.1$  L/min throughout the implantation period.

The protrusions resembling those of the sinus of Valsalva did not significantly change in size or shape within the 1-month period after implantation [Figure 6(F)]. All blood contact surfaces, including the luminal surface of the conduit and leaflet surfaces, were white and had minimal visible thrombus formation [Figures 6(F, G)]. The leaflets did not show any evidence of structural damage.

Histological examination showed consistent wall thicknesses in the Biovalves, prior to implantation, at the conduit ( $287.5 \pm 33.1$   $\mu\text{m}$ ) and leaflet parts ( $350.0 \pm 58.0$   $\mu\text{m}$ ); however, the wall was slightly thinner at the sinus of Valsalva ( $202.5 \pm 31.1$   $\mu\text{m}$ ) [Figure 7(A)]. The main component of the Biovalves was collagen, which stains blue with Masson's trichrome stain [Figure 7(E)], and a minimal amount of elastic fiber [Figure 7(D)]; the cellular components were also minimal [Figure 7(B)]. Both surfaces of the leaflets were very smooth.

After implantation, the wall thickness of the leaflet membrane was generally well maintained ( $332.3 \pm 82.5$   $\mu\text{m}$ ), whereas the thickness at the sinus of Valsalva decreased ( $<100$   $\mu\text{m}$ ); however, at the sinus of Valsalva, there was a thick lining of connective tissue that had migrated from the surrounding tissue [Figure 7(E)]. The remaining tissues consisted of extracellular matrix, which remained predominantly collagenous [Figures 7(G, H)]. Minimal cell ingrowth was evident [Figure 7(F)].

#### DISCUSSION

The technology used in this report required several months to produce the tissue prostheses. However, a management process, including cell incubation, was not required for during the tissue formation period. The implantable, autologous tissues were naturally formed according to the shape of the

TABLE I. Comparison of Several Types of Biovalves



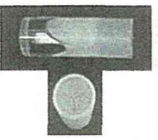





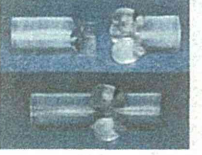

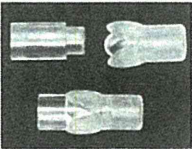

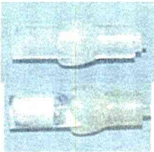

Type	Mold and Its Materials	Embedding Into	Biovalve and Its Composition	Implantation Into	Characteristics and Problems	References
I	 SI rod covered with PU sponge crown	Rabbit	 AT crown-shaped PU	na	Aortic valve replacement type. Mechanical properties of Biovalve leaflets were statistically equivalent to those of porcine ones. PU was remained in Biovalve.	11
II	 Assembly of concave SI rod and convex AC rods (upper), covered with PU sponge tube (lower)	Rabbit	 AT PU tube	na	Conduit type. PU was remained in Biovalve.	18
III	 AT connective tissue-covered SI rod partially rapped with PU tubular sheet	Rabbit	 AT	na	Conduit type by completely autologous tissue without any artificial material. Two-times in-body tissue architecture process was needed.	19
IV	 Assembly of concave and convex SI rods (upper), covered with PU mesh tube (lower)	Rabbit	 AT Tubular PU mesh	na	Conduit type with the sinus of Valsalva. PU was remained in Biovalve.	20
V	 Concave and convex-shaped SI rods (upper) and their assembly (lower)	Beagle dog	 AT	Beagle dogs as a pulmonary valve (84 days)	Completely autologous conduit type tissue with the sinus of Valsalva. The three commissures had large aperture depending on the mold design. Before implantation suturing of the apertures was needed to avoid regurgitation.	10



TABLE I. Continued

Type	Mold and Its Materials	Embedding Into	Biovalve and Its Composition	Implantation Into	Characteristics and Problems	References
VI	 Concave AC rod by 3D printer and convex SI rod (upper), and their assembly (lower)	Goat	 AT	Goats as an aortic valve (2 months)	Completely autologous conduit type tissue with the sinus of valsalva. Low regurgitation rate (12.7%) and high opening ratio (ca. 50%) by leaflet formation at its open position. The size of Valsalva was limited to low to avoid tissue damage at mold removing process.	12 and 21
VII	 Assembly of AC parts by 3D printer (upper) and with capsule endoscope (lower)	Goat	 AT	Goats as an aortic valve (1 month)	Completely autologous conduit type tissue with the sinus of valsalva similar to native shape and size. Extremely low regurgitation rate (<3%). The mold parts could be removed by step-by-step separation from the formed Biovalve without any tissue damage.	22

Abbreviations: SI, silicone; PU, polyurethane; AC, acrylate; AT, autologous tissue.

molds. This technology has been previously used for the development of cardiovascular tissues with vascular grafts, namely Biotubes.<sup>13,15</sup> The Biotubes were formed within a relatively short period (4 weeks) after embedding rod-like molds into subcutaneous pouches because the whole mold surfaces were attached directly to the subcutaneous tissue. In comparison, since tissue migration into a small aperture is slow, leaflet formation in the Biovalves took longer, following the formation of the conduit. Therefore, in this study, non-invasive ECs were impregnated into the molds to confirm complete leaflet tissue formation, before harvesting. The formation process with a success rate of 90% could be clearly observed [Figure 2(C)]. If stronger materials were selected for the mold parts and if sterile conditions were more strictly controlled, a success rate of nearly 100% could be obtained. Furthermore, another advantage of the mold developed in this study was their prefabrication. Although the Biovalves had three projections, mimicking the sinus of Valsalva, the internal molds were easily removed and separated, due to the use of 3D digital printer-based molding.

The wall thicknesses of the conduit and leaflet parts of the Biovalves were almost the same (approximately 300  $\mu\text{m}$ ). However, the tensile strengths of the two parts were quite different. The tensile strength of conduit tissue was three times stronger than that of the leaflet, which was approximately equivalent to that of a natural goat leaflet. As the main component of both parts was collagen, we believe that the difference in the strength was depended on the density or orientation of the collagen fibers. The conduit part was formed around a rod. Thus, the collagen membrane formation process involved collagen fibers that may have pulled each other to completely cover the rod. This may have resulted in a higher density and better organization of the collagen fibers, leading to greater strength. On the other hand, the leaflet was formed in a small aperture between the sections of the mold. The collagen filled only the aperture, with little mechanical stimulation. This may have resulted in a lower strength of the tissue formed. In a separate study, we are developing a scanning haptic microscope that can observe the precise distribution of the elastic modulus on a cross-sectional surface of the tissue.<sup>16,17</sup> This is accomplished by segregating the elastin-rich and collagen-rich areas on the aortic tissue. Therefore, the differences in the density or the orientation of the collagen fibers, between the conduit and leaflet parts, will be obvious.

The leaflet thickness of human or goat aortic valves is about 200  $\mu\text{m}$ , which is about 60% of that of the leaflets of the developed Biovalve. The thickness of the Biovalve leaflets depended on the thickness of the aperture in the molds for Biovalve preparation. In our preliminary examination for this study, in thin aperture less, tissue ingrowth was strongly inhibited. Therefore, to obtain thin leaflet as possible we selected the aperture thickness of 500  $\mu\text{m}$ .

The encapsulating connective tissue was confirmed to be effective for use as leaflet tissue in heart valves in the first generation of Biovalve, developed in 2007.<sup>11</sup> The comparison of the several types of Biovalves is summarized in

Table I. After repeated improvements, the type V pulmonary Biovalve was successfully used in a beagle dog model in 2010.<sup>10</sup> However, the major disadvantage of that Biovalve was the structure of the leaflet mold, which resulted in considerable regurgitation. The three commissures between the leaflets had an aperture of approximately 1 mm. To avoid regurgitation, the apertures had to be sutured prior to implantation, which could potentially limit the Biovalve durability, particularly in systemic circulation. In the type VI Biovalve, the trileaflets were created in an open form, allowing the commissures to be connected without an aperture.<sup>12</sup> This resulted in a reduction in the regurgitation rate of 12.7%, while maintaining a high opening ratio of approximately 50%. The most recently improved Biovalve (Biovalve VII) involves a novel mold created using a 3D printer, yielding three projections that resemble the native sinuses of Valsalva in both shape and size. The vortex flow in the sinus of Valsalva plays an important role in the closure of the native semilunar valves and in the overall coronary flow. This version of the Biovalve showed excellent valvular function, with an extremely low regurgitation rate of <3%.

A fundamental requirement for the long-term performance of aortic heart valve leaflets is a dense, organized collagen matrix.<sup>23</sup> Based on the property of anisotropy, this matrix should, ideally, be developed prior to implantation. This study indicates that autologous *in vivo* tissue-engineered heart valves are promising aortic valve replacements, having minimal regurgitation in systemic circulation. Since Biovalves consist of a dense collagen matrix, valvular function was maintained for 10 days, even in saline. Moreover, the *in vivo* collagen matrix was retained despite unfavorable implantation conditions in the apico-aortic bypass method, in which the Biovalves were isolated from the native cardiovascular tissues by the interposition of artificial vascular grafts. In addition, the whole luminal surface was extremely smooth and well contoured, without any thrombus formations, despite the lack of endothelialization. These results indicate that the newly formed collagen in the Biovalves was robust and compatible with blood, suggesting that culturing, seeding, and conditioning autologous cells on a scaffold, as required for the creation of *in vitro* tissue-engineered valves, may be unnecessary. If Biovalves are used as anatomic aortic valve replacements, tissue ingrowth, including complete endothelialization, is expected. This would be similar to that demonstrated in the previous studies of pulmonary valve replacement with Biovalves<sup>10</sup> or the vascular implantation of Biotubes.<sup>12,15</sup>

## CONCLUSION

3D printing was successfully demonstrated to be useful in the fabrication of the fine components required to create Biovalve molds. Biovalves, with sinuses of Valsalva, obtained from the mold satisfied the highly specialized systemic circulation requirements *in vitro* and *in vivo*. The Biovalve developed in this study is a conduit-type structure, which clinically needs an aortic root implant with reimplantation of the coronary ostia. We further aim to create a Biovalve

without a sinus of Valsalva conduit that is suitable for traditional aortic valve replace (AVR). We also aim to develop a Biovalve that is suitable for transcatheter AVR (TAVR), involving a valve leaflet construct that is connected/fixed to an expanding stent. In a previous study, metallic stents, covered with an autologous membranous tissues, were developed by applying this "in-body tissue architecture technology" to create Biocovered stents.<sup>24</sup> Using this method, Biovalves for use in both AVR and TAVR devices are under development.<sup>25</sup> We strongly believe that Biovalves have the potential to overcome the limitations of the currently used bioprosthetic valves, which are inherently prone to dysfunctional calcification and degeneration. This application may broaden future clinical opportunities for valve replacements. Biovalves do not require special handling techniques, either by the hospital staff or by the surgeon, thus facilitating their usage.

#### ACKNOWLEDGMENTS

The authors thank Ms. Manami Sone for her participation in this study.

#### REFERENCES

1. Le Tourneau T, Savoye C, McFadden EP, Grandmougin D, Carton HF, Hennequin JL, Dubar A, Fayad G, Warembourg H. Mid-term comparative follow-up after aortic valve replacement with Carpentier-Edwards and Pericardion pericardial prostheses. *Circulation* 1999;100(19 Suppl):II11-1116.
2. Gandaglia A, Bagno A, Naso F, Spina M, Gerosa G. Cells, scaffolds and bioreactors for tissue-engineered heart valves: A journey from basic concepts to contemporary developmental innovations. *Eur J Cardiothorac Surg* 2011;39:523-531.
3. Berry JL, Steen JA, Koudy Williams J, Jordan JE, Atala A, Yoo JJ. Bioreactors for development of tissue engineered heart valves. *Ann Biomed Eng* 2010;38:3272-3279.
4. Webb PA. A review of rapid prototyping (RP) techniques in the medical and biomedical sector. *J Med Eng Technol* 2000;24:149-153.
5. Curodeau A, Sachs E, Caldarise S. Design and fabrication of cast orthopedic implants with freeform surface textures from 3-D printed ceramic shell. *J Biomed Mater Res* 2000;53:525-535.
6. Gagg G, Ghassemieh E, Wiria FE. Effects of sintering temperature on morphology and mechanical characteristics of 3D printed porous titanium used as dental implant. *Mater Sci Eng C Mater Biol Appl* 2013;33:3858-3864.
7. Butscher A, Böhner M, Doeblin N, Hofmann S, Müller R. New depowdering-friendly designs for three-dimensional printing of calcium phosphate bone substitutes. *Acta Biomater* 2013;9:9149-9158.
8. Hockaday LA, Kang KH, Colangelo NW, Cheung PY, Duan B, Malone E, Wu J, Girardi LN, Bonassar LJ, Lipson H, Chu CC, Butcher JT. Rapid 3D printing of anatomically accurate and mechanically heterogeneous aortic valve hydrogel scaffolds. *Biofabrication* 2012;4:035005; doi:10.1088/1758-5082/4/3/035005.
9. Meseguer-Olmo L, Vicente-Ortega V, Alcaraz-Baños M, Calvo-Guirado JL, Vallet-Regi M, Arcos D, Baeza A. In-vivo behavior of Si-hydroxyapatite/polycaprolactone/DMB scaffolds fabricated by 3D printing. *J Biomed Mater Res Part A* 2013;101A:2038-2048.
10. Yamanami M, Yahata Y, Uechi M, Fujiwara M, Ishibashi-Ueda H, Kanda K, Watanabe T, Tajikawa T, Ohba K, Yaku H, Nakayama. Development of a completely autologous valved conduit with the sinus of Valsalva using in-body tissue architecture technology: A pilot study in pulmonary valve replacement in a beagle model. *Circulation* 2010;122(11 Suppl):S100-S106.
11. Hayashida K, Kanda K, Yaku H, Ando J, Nakayama Y. Development of an in vivo tissue-engineered, autologous heart valve (the biovalve): Preparation of a prototype model. *J Thorac Cardiovasc Surg* 2007;134:152-159.
12. Nakayama Y, Yahata Y, Yamanami M, Tajikawa T, Ohba K, Kanda K, Yaku H. A completely autologous valved conduit prepared in the open form of trileaflets (type VI biovalve): Mold design and valve function in vitro. *J Biomed Mater Res B Appl Biomater* 2011;99:135-141.
13. Nakayama Y, Ishibashi-Ueda H, Takamizawa K. In vivo tissue-engineered small-caliber arterial graft prosthesis consisting of autologous tissue (biotube). *Cell Transplant* 2004;13:439-449.
14. Gheorghe C, Iacob R, Bancila I. Olympus capsule endoscopy for small bowel examination. *J Gastrointest Liver Dis* 2007;16:309-313.
15. Watanabe T, Kanda K, Yamanami M, Ishibashi-Ueda H, Yaku H, Nakayama Y. Long-term animal implantation study of biotube-autologous small-caliber vascular graft fabricated by in-body tissue architecture. *J Biomed Mater Res B Appl Biomater* 2011;98:120-126.
16. Moriwaki T, Oie T, Takamizawa K, Murayama Y, Fukuda T, Omata S, Kanda K, Nakayama Y. Variations in local elastic modulus along the length of the aorta as observed by use of a scanning haptic microscope (SHM). *J Artif Organs* 2011;14:276-283.
17. Oie T, Suzuki H, Murayama Y, Fukuda T, Omata S, Kanda K, Takamizawa K, Nakayama Y. Surface elasticity imaging of vascular tissues in a liquid environment by a scanning haptic microscope. *J Artif Organs* 2010;13:121-125.
18. Hayashida K, Kanda K, Oie T, Okamoto Y, Ishibashi-Ueda H, Onoyama M, Tajikawa T, Ohba K, Yaku H, Nakayama Y. Architecture of an in vivo-tissue engineered autologous conduit "Biovalve". *J Biomed Mater Res B Appl Biomater* 2008;86:1-8.
19. Nakayama Y, Yamanami M, Yahata Y, Tajikawa T, Ohba K, Watanabe T, Kanda K, Yaku H. Preparation of a completely autologous trileaflet valve-shaped construct by in-body tissue architecture technology. *J Biomed Mater Res B Appl Biomater* 2009;91:813-818.
20. Yamanami M, Yahata Y, Tajikawa T, Ohba K, Watanabe T, Kanda K, Yaku H, Nakayama Y. Preparation of in-vivo tissue-engineered valved conduit with the sinus of Valsalva (type IV biovalve). *J Artif Organs* 2010;13:106-112.
21. Takewa Y, Yamanami M, Kishimoto Y, Arakawa M, Kanda K, Matsui Y, Oie T, Ishibashi-Ueda H, Tajikawa T, Ohba K, Yaku H, Taenaka Y, Tatsumi E, Nakayama Y. In vivo evaluation of an in-body, tissue-engineered, completely autologous valved conduit (biovalve type VI) as an aortic valve in a goat model. *J Artif Organs* 2013;16:176-184.
22. Sumikura H, Nakayama Y, Ohnuma K, Takewa Y, Tatsumi E. In vitro evaluation of a novel autologous aortic valve (biovalve) with a pulsatile circulation circuit. *Artif Organs* 2014;38:282-289.
23. Mol A, Rutten MC, Driessen NJ, Bouten CV, Zünd G, Baaijens FP, Hoerstrup SP. Autologous human tissue-engineered heart valves: Prospects for systemic application. *Circulation* 2006;114(1 Suppl):I152-I158.
24. Nakayama Y, Zhou YM, Ishibashi-Ueda H. Development of in vivo tissue-engineered autologous tissue-covered stents (biocovered stents). *J Artif Organs* 2007;10:171-176.
25. Mizuno T, Takewa Y, Sumikura H, Ohnuma K, Moriwaki T, Yamanami M, Oie T, Tatsumi E, Uechi M, Nakayama Y. Preparation of an autologous heart valve with a stent (stent-biovalve) using the stent eversion method. *J Biomed Mater Res B Appl Biomater*. Forthcoming.



# Occlusion of canine aneurysms using microporous self-expanding stent grafts: Long-term follow-up

Shogo Nishi<sup>a,\*</sup>, Yasuhide Nakayama<sup>b</sup>, Hatsue Ishibashi-Ueda<sup>c</sup>, Yoshida Masato<sup>d</sup>

<sup>a</sup> Department of Neurosurgery, Interventional Neurosurgery, Spinal Surgery, Sapporo-Higashi Tokushukai Hospital, Sapporo, Hokkaido, Japan

<sup>b</sup> Department of Bioengineering, Advanced Biomedical Engineering Center, National Cerebral and Cardiovascular Center Research Institute, Suita, Osaka, Japan

<sup>c</sup> Department of Pathology, National Cerebral and Cardiovascular Center Hospital, Suita, Osaka, Japan

<sup>d</sup> Department of Neurosurgery, Nozaki Tokushukai Hospital, Osaka, Japan

## ARTICLE INFO

### Article history:

Received 29 January 2014

Received in revised form 12 April 2014

Accepted 14 April 2014

Available online 22 April 2014

### Keywords:

Microporous self-expanding stent graft

Canine experimental aneurysms

Hybrid stent grafts

Covered stents

Long-term follow-up

## ABSTRACT

**Purpose:** The treatment of large or giant cerebral aneurysms by surgical and/or endovascular techniques is difficult and poses relatively high risks. Therefore, a microporous self-expanding (hybrid) stent graft composed of a thin, expandable, segmented polyurethane (SPU) membrane with micropores and a drug-delivery system was developed.

**Materials and methods:** A commercially available, self-expanding carotid stent was covered with a thin microporous SPU membrane fabricated by the dip-coating method and the excimer laser ablation technique, with an intraluminal coating of argatroban. Experimentally fabricated lateral-wall aneurysms in canine carotid arteries using venous pouches were occluded with the hybrid stent graft (bale-shaped pore density of 23.6%) on one side and a bare-metal stent on the other side without systemic antiplatelet therapy.

**Results:** Angiography at 1, 6, and 12 months of stenting revealed that all arteries were patent without marked stenosis without systemic antiplatelet therapy. All aneurysms treated with hybrid stent grafts remained occluded throughout the 12-month period, while among those treated by bare-metal stents, 2 of 3 aneurysms were occluded at 6 months (67%) and only 1 of 3 aneurysms were occluded at 12 months (33%). Histology revealed that the novel hybrid stent graft had less intimal hyperplasia than the bare-metal stent. The hybrid stent graft was useful for the successful occlusion of these canine carotid aneurysms, even at 12 months.

**Conclusions:** The novel hybrid stent grafts are expected to overcome the disadvantages of fully covered stent grafts and simple bare-metal stents, while combining both their merits, and appear to be useful in the treatment of large or giant cerebral aneurysms.

© 2014 Elsevier B.V. All rights reserved.

## 1. Introduction

Large, giant, or dissecting aneurysms with a broad neck occurring in the craniocervical area are difficult to treat surgically and/or endovascularly. The surgical treatment of such aneurysms involves direct aneurysm neck clipping [1,2], aneurysm trapping, proximal occlusion of the parent artery with or without a bypass [3], or a combination of clipping with coiling or a bypass [4]; endovascular treatment involves bare-metal, balloon-expandable, or self-expanding stent-assisted coiling [5–8]; use of simple covered stents [9,10]; use of flow-diverter stents [11–13]; or parent

artery occlusion or trapping with or without a bypass [14,15]. Stent treatment is based on the assumption that the metallic struts induce alterations in the blood flow dynamics within an aneurysm, thereby inducing and promoting thrombus formation and fibrosis within the residual aneurysmal lumen [16,17]. However, aneurysms treated with stenting may be prone to recanalization or parent artery stenosis due to neo-intimal proliferation [18].

The recently developed pipeline embolization device (PED) is a self-expanding cylindrical mesh device with 48 individual cobalt chromium and platinum strands having 30–35% metal surface coverage, intended to be porous enough to preserve the patency of any branch vessels requiring coverage [11].

Microporous, self-expanding stent grafts have been developed for the occlusion of cerebral aneurysms, particularly extracranial and vertebrobasilar aneurysms. The newly developed stent graft is a hybrid of a bare-metal stent and a fully covered stent created by

\* Corresponding author at: Department of Neurosurgery, Neuro-Intervention, Spinal Surgery, Sapporo Higashi-Tokushukai Hospital 14-3-1, Higashi, N33, Higashi-ku, Sapporo, Hokkaido 065-0033, Japan. Tel.: +81 11 722 1110; fax: +81 11 722 0378.  
E-mail address: [nishi@higashi-tokushukai.or.jp](mailto:nishi@higashi-tokushukai.or.jp) (S. Nishi).



adjusting the porosity of the covering film, with a thin, expandable segmented polyurethane (SPU) membrane; micropores created by the excimer laser ablation technique for regulating endothelialization and intimal invasion; and a drug-delivery system at the membrane [19–21]. The present study examines the long-term occlusion efficacy of the experimentally fabricated hybrid stent in the treatment of canine carotid aneurysms.

## 2. Methods

### 2.1. Animals

For this study, experimental aneurysms were created in the carotid arteries of 12 female beagles (age, 12 months; weight, 13–15 kg). One month after aneurysm formation, each animal underwent placement of the novel microporous self-expanding stent graft in the carotid aneurysm of one side and a bare-metal self-expanding stent, on the other. Angiography was performed at 1, 6, and 12 months after stenting. Histological examination was performed after euthanizing the animals.

All animal experiments were performed in the acute setting under sterile conditions, in compliance with the Principles of Laboratory Animal Care (formulated by the National Society for Medical Research, Chicago, IL) and the Guide for the Care and Use of Laboratory Animals (NIH publication no. 86-23, revised 1985; National Institute of Health, Bethesda, MD). The research protocol (no. 09043) was approved by the ethics committee of the National Cerebral and Cardiovascular Center Research Institute.

### 2.2. Fabrication of aneurysms

Bilateral experimental side-wall carotid aneurysms were created in the carotid arteries of 12 female beagles by end-to-side anastomosis using an autologous venous pouch, as described previously [19–21]. The aneurysms measured approximately 5 mm in diameter at the neck and 10 mm in length. All procedures were performed under general anesthesia. The beagles were transmuscularly premedicated with ketamine chloride (dose range, from 150 mg/3 mL to 250 mg/5 mL per beagle), intubated endotracheally, and anesthetized with an intravenous administration of sodium pentobarbital at 50 mg/1 mL or 100 mg/2 mL according to the active motion. The carotid arteries and right external jugular vein on both sides were exposed under sterile conditions, and 2 venous pouches were created by one-sided ligation with threads after the harvesting of the right external jugular vein. The carotid artery and the venous pouch were anastomosed (side-to-end anastomosis) with discontinuous 7-0 nylon sutures, while the artery was temporarily clamped. After removing the clamp, the bleeding was controlled by additional suturing or local compression. The necks of the aneurysm were marked with radiopaque strings. After awakening from anesthesia, the dogs were allowed ad libitum access to food.

### 2.3. Fabrication of stent grafts

Bare-metal, self-expanding stents (Luminexx stents: diameter, 5 mm; length, 20 mm; Brad Inc., Murray Hill, NJ) taken out from their primary delivery systems were coated with an SPU film (Miractran, Tokyo, Japan) by dipping them in a tetrahydrofuran solution when sealed on a stainless mold (diameter, 5 mm). The thickness of the film was restricted to approximately 50  $\mu\text{m}$ . Micropores were then created in the cover film by using a KrF excimer laser apparatus (L4500; Hamamatsu Photonics, Shizuoka, Japan). We created a bale-shaped pore type, with a pore size and interpore distance of  $100 \times 268 \mu\text{m}$  and  $250 \mu\text{m}$ , respectively, to achieve an opening ratio of 23.6% (Fig. 1). The control stent comprised a bare-metal stent with an opening ratio of 86%. The

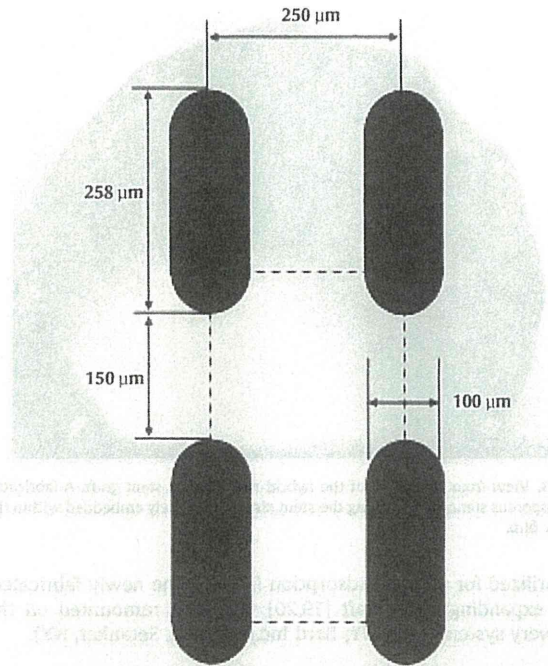


Fig. 1. Schema of the pore design. Pore diameter and the interpore distance were  $100 \times 268 \mu\text{m}$  and  $250 \mu\text{m}$ , respectively, with an opening ratio of 23.6% (bale-shaped); the circumference at the 5-mm diameter was 15.7 mm.

outer surface of the SPU film of the microporous stent grafts was coated with argatroban ( $500 \mu\text{g}/\text{cm}^2$ ), which was applied using a methanol solution (1% w/v); the solvent was subsequently

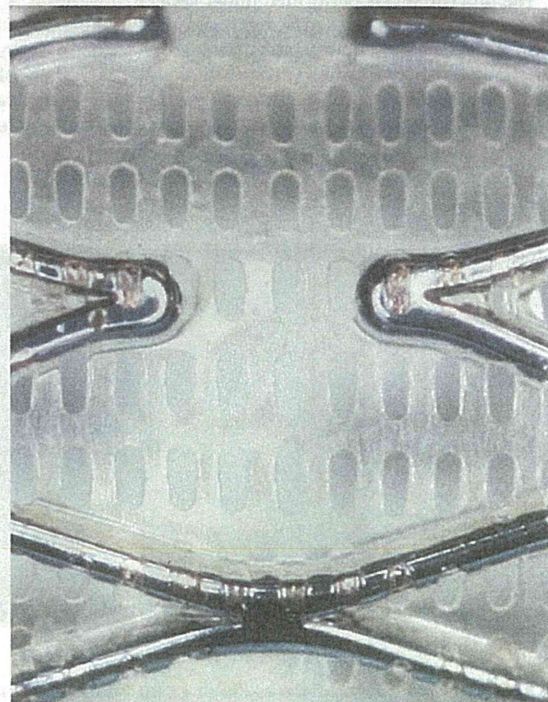
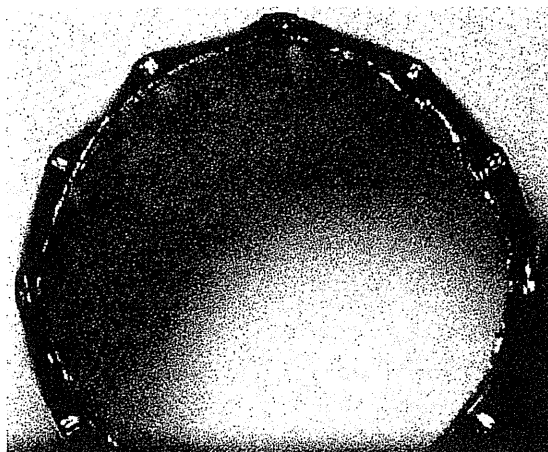


Fig. 2. Pore design in the hybrid microporous stent graft. Post-fabrication microporous stent graft showing bale-shaped micropores before remounting.



**Fig. 3.** View from either end of the hybrid microporous stent graft. A fabricated microporous stent graft showing the stent struts completely embedded within the cover film.

volatilized for physical adsorption (Fig. 2). The newly fabricated, self-expanding stent graft [19,20] was then remounted on the delivery system (6 or 7 Fr; Bard Inc./Medicon, Setauket, NY).

#### 2.4. Intravascular procedures

One month after aneurysm creation, the neck of each aneurysm was sealed with the prepared microporous stent grafts or bare-metal stents ( $n = 12$  each). Overall, 2 stent grafts and 1 bare-metal stent had not been implanted (as they had been scheduled for implantation at 1 and 6 months, respectively, after the creation of the aneurysms) owing to the inadequate size of the formed aneurysms.

The procedure was performed under general anesthesia. A 7-Fr delivery system comprising the microporous self-expanding stent graft or bare-metal stent was introduced into the sheath, navigated into the affected carotid artery, and positioned across the neck of the aneurysm under fluoroscopic guidance. The stent was then released at this site. Angiography was subsequently performed to evaluate the

status of the treated aneurysm and the parent artery. All dogs recovered from anesthesia without complications and were followed up without administering systemic antiplatelet therapy.

#### 2.5. Histological procedure

Angiography was performed 1, 6, and 12 months after stenting. Histological examination was performed after euthanasia, by using a cross-sectional sample (30–40  $\mu\text{m}$  in thickness) from the stented portion of the aneurysms.

#### 2.6. Statistical analysis

Patency of the parent arteries was analyzed using Fisher's exact test. Measurements of intimal thickness at 8 points, i.e., at every 45° in the transverse section, were analyzed using repeated-measures analysis of variance (ANOVA).

### 3. Results

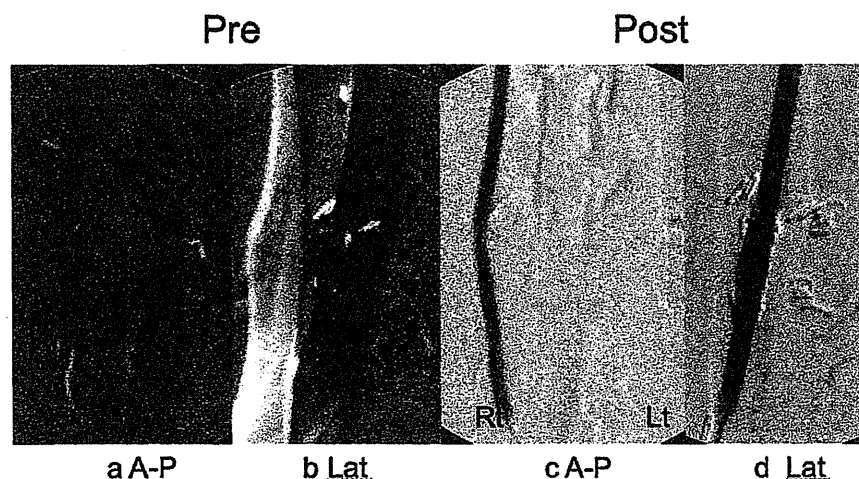
#### 3.1. Remounting

The self-expanding stents were successfully fabricated, and the micropores were noted to uniformly cover the film. The stent struts were completely embedded within the cover film (Fig. 3). The shape of the expanded stent graft and its mechanical properties, such as the flexibility of the cover film, remained unchanged, irrespective of the nature of the covering or the degree of porosity [20]. The stent grafts could be shrunk by using a hand-held crimping device without any damage to the cover film [19]. Further, the remounting procedure was easily performed using the standard endoscopic method [19].

#### 3.2. Stenting

Bilateral side-wall carotid aneurysms were created in each animal, requiring approximately 2 h from premedication for anesthesia to wound closure.

One month after aneurysm creation, stenting procedures were performed without any technical difficulties, requiring approximately 30 min per animal. The insertion of the self-expanding stent



**Fig. 4.** Right carotid arteriogram shows an experimentally constructed lateral-wall aneurysm occluded by a microporous, self-expanding stent graft. Anteroposterior and lateral control arteriograms show a broad-based lateral-wall aneurysm of the right common carotid artery (approximate diameter of the parent vessel: 4.5 mm) (a, b). Angiogram performed immediately (c, d) after introduction of a microporous self-expanding stent graft shows complete occlusion of the aneurysm. Abbreviations: A-P, anteroposterior projection; Lat, lateral projection; Rt, Right; Lt, Left.



grafts was performed as smoothly as that of the control bare-metal self-expanding stents. Occlusion of the aneurysms was achieved immediately or some minutes after stenting, without the need for post-dilation.

In 3 of the experimental animals, the aneurysm formed in one of the carotid arteries was found to have occluded naturally before the stenting procedure. Therefore, occlusion of the aneurysm—using a self-expanding stent graft scheduled at 1-month follow-up or a bare-metal self-expanding stent scheduled at 3-month follow-up—was not performed. These 3 carotid sides were excluded from analysis in this study.

### 3.3. Angiography

As mentioned previously, 2 stent grafts and 1 bare-metal stent had not been implanted (as they had been scheduled for implantation at 1 and 6 months, respectively, after the creation of the aneurysms) owing to the inadequate size of the formed aneurysms.

Angiography performed at 1, 6, and 12 months after occlusion by stenting revealed that for the self-expanding stent graft, all the aneurysms were completely occluded without significant parent artery stenosis (100%, 10/10 animals; excluding the 2 animals in which stent implantation was not performed as described above) at all time points, without systemic antiplatelet therapy. For the bare-metal stents, however, the aneurysms were occluded only in some cases: no occlusion in 5 aneurysms at 1 month, occlusion in 2 of 3 aneurysms (67%; excluding 1 animal in which stenting was not performed as described above) at 6 months (Figs. 4 and 5), and occlusion in 1 of 3 aneurysms (33%) at 12 months (Figs. 6 and 7); thus, on an average, occlusion was observed only in 3 of 11

aneurysms (27%) across all time points (Table 1). The patency of the parent arteries in the sites implanted with self-expanding stent grafts was markedly higher than that in the sites implanted with bare-metal stents. Fisher's exact test showed significant differences on aneurysmal occlusion between the hybrid self-expanding stent grafts and bare-metal stents through all intervals ( $p < 0.001$ ).

### 3.4. Histology

Histological examination at 1, 6 (Fig. 8a), and 12 (Fig. 9a) months after implantation of the stent grafts revealed that the aneurysms were packed with granulomatous tissues and that the luminal surface of the neck was covered with a thin layer of fibrous tissue and endothelial cells. At 6 (Fig. 8b) and 12 (Fig. 9b) months after implantation of the bare-metal stents, some of the aneurysms were packed with similar granulomatous tissues, and the luminal surface of the neck was covered with similar fibrous tissue and endothelial cells. Thus, irrespective of the type of stent used, once occluded, the aneurysms were packed with organized tissues.

The intimal thickness in the self-expanding stent grafts tended to be lower than that in the bare-metal stents (Fig. 10). Repeated-measures ANOVA showed significant differences between the hybrid self-expanding stent grafts and bare-metal stents at each interval ( $1879 \pm 390 \mu\text{m}$ , at 1 month ( $n=3$ ,  $p < 0.0001$ );  $3196 \pm 1424 \mu\text{m}$ , at 6 months ( $n=4$ ,  $p < 0.0141$ ); and  $2261 \mu\text{m} \pm 344 \mu\text{m}$ , at 12 months ( $n=3$ ,  $p < 0.0001$ ) vs  $3398 \pm 756 \mu\text{m}$ , at 1 month ( $n=5$ );  $4004 \pm 516 \mu\text{m}$ , at 6 months ( $n=3$ ); and  $3974 \pm 284 \mu\text{m}$  at 12 months ( $n=3$ ), respectively). However, no statistically significant differences were noted in the intimal

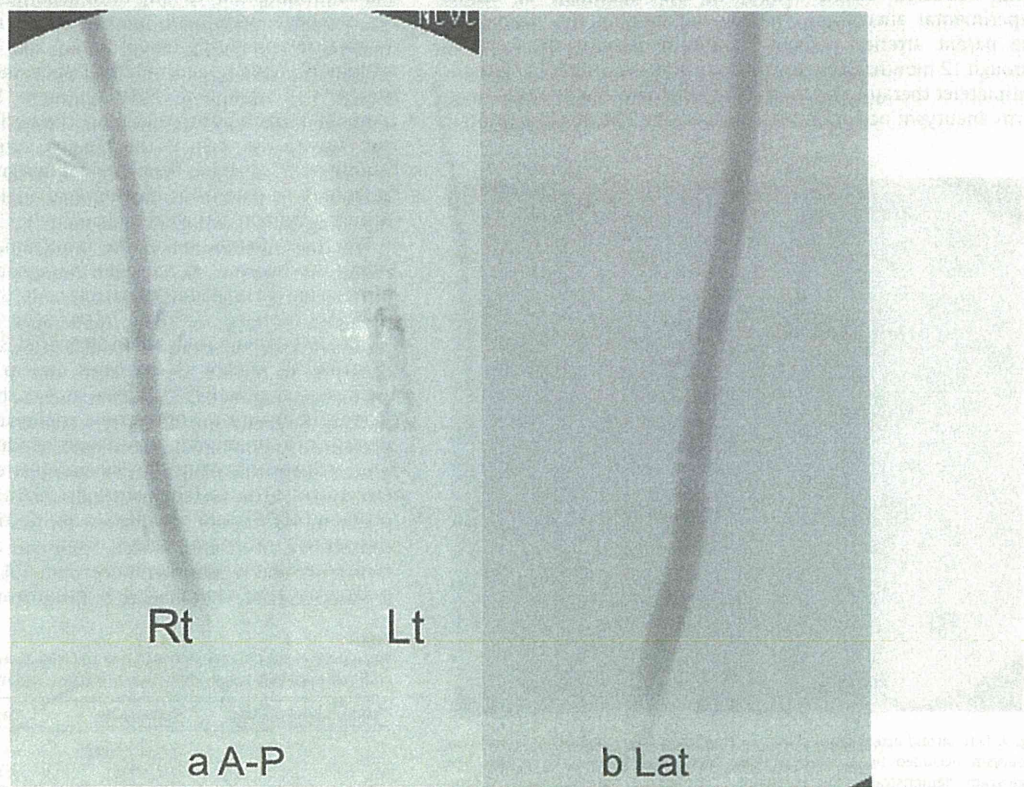


Fig. 5. Angiogram at 6 months after implantation of the microporous self-expanding stent graft. The aneurysm remained occluded without any significant narrowing of the parent vessel (a: anteroposterior view, b: lateral view). Abbreviations: A-P, anteroposterior projection; Lat, lateral projection; Rt, Right; Lt, Left.



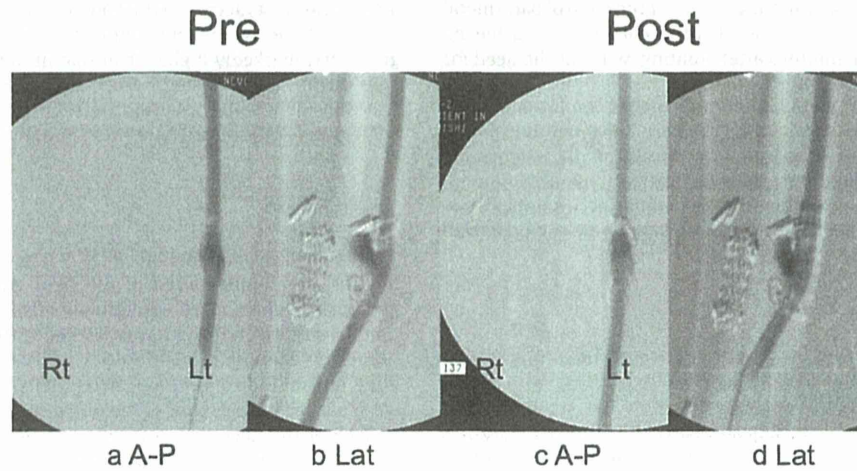


Fig. 6. Left carotid arteriogram shows an experimentally constructed lateral-wall aneurysm occluded by a self-expanding bare-metal stent. Anteroposterior and lateral control arteriogram shows a broad-based lateral-wall aneurysm of the left common carotid artery (approximate diameter of the parent vessel: 5 mm) (a, b). Angiogram performed immediately (b) after transfemoral placement of a self-expanding stent shows complete patency of the aneurysm with the patent parent vessel. Abbreviations: A-P, anteroposterior projection; Lat, lateral projection; Rt, Right; Lt, Left.

hyperplasia across different time periods for the hybrid stent grafts and bare-metal stents ( $p = 0.1986$ ).

#### 4. Discussion

The newly developed hybrid self-expanding stent graft with micropores and argatroban coating demonstrated successful long-term occlusion effects (100%) in the treatment of canine experimental aneurysms, thereby maintaining the patency of the parent arteries without significant stenosis or occlusion through 12 months of aneurysm occlusion, even without systemic antiplatelet therapy. Moreover, even with bare-metal stents, long-term aneurysm occlusion was observed in 27% of cases (3 of 11

aneurysms). Further, 2 stent grafts and 1 bare-metal stent had not been implanted, as they had been scheduled for implantation at 1 month and 6 months, respectively.

The microporous membrane fabricated for this hybrid stent has been previously shown to induce early endothelialization and subsequent secretion of tissue plasminogen [22] only 1 week after stent graft implantation [21], thereby avoiding early thrombosis and controlling mid- to long-term hyperplasia [23]. Polyurethane has excellent elastomeric properties and is clinically used as a material for preparing blood pumps and arterial grafts; it also exhibits no toxicity and minimal biodegradation [24–26]. Argatroban, an arginine-derived synthetic low-molecular-weight compound that binds to thrombin, competitively inhibits fibrinogen cleavage as well as the platelet activation stimulated by thrombin [27,28]. It has been used for designing antithrombogenic surfaces in percutaneous transluminal angioplasty (PTA) devices, including balloon catheters and stents [29,30].

For the embolization of the intracranial aneurysmal lumen, coiling has become an accepted therapeutic modality since the introduction of Guglielmi detachable coils [31]. However, complete occlusion of large or giant intracranial aneurysms with this technique is obtained only in 10–68% cases [32], with recanalization occurring in 56–90% of the cases due to coil compaction and aneurysmal regrowth [33]. Factors such as the difficulties in tightly packing the aneurysm, the coil type, aneurysm morphology, and the presence of a thrombus in the aneurysm induce recurrence in large, giant, or dissecting aneurysms. For example, recanalization requiring retreatment is the least for hydrocoils (26.6%), intermediate for bare platinum (43.7%), and the highest for Matrix type (65.2%) in 100 consecutive, 4–15 mm, coiled, ruptured aneurysms [34]. The recurrence and retreatment rates were 39% and 33%, respectively, for large or giant, wide-necked or fusiform aneurysms in 334 cases

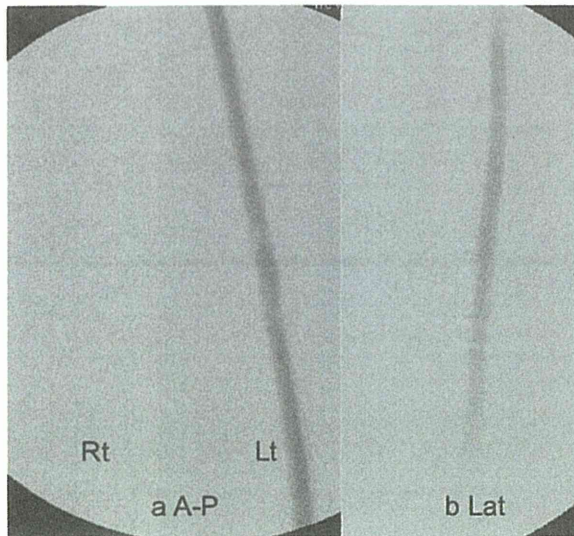


Fig. 7. Left carotid arteriogram shows an experimentally constructed lateral-wall aneurysm occluded by a self-expanding bare-metal stent at 6 months. The angiogram demonstrates the complete occlusion of the aneurysm without significant narrowing of the parent vessel (a: anteroposterior view, b: lateral view). Abbreviations: A-P, anteroposterior projection; Lat, lateral projection; Rt, Right; Lt, Left.

Table 1

The patency of the parent arteries in the sites implanted with self-expanding stent grafts was markedly higher than that in the sites implanted with bare-metal stents.

Follow-up (months)	Stent grafts	Bare-metal stents	Total
1	3/3(–2)(100%)	0/5(0%)	5
6	4/4(100%)	2/3(–1)(67%)	4
12	3/3(100%)	1/3(33%)	3
Total	10/10(–2)(100%)	3/11(–1)(27%)	12

\*  $p < 0.001$ .